Computational method for simulation of eccentric annular displacements of non-Newtonian fluids

S. Pelipenko

Etudes et Productions Schlumberger, 1, rue Becquerel, 92140 Clamart - France.

I.A. Frigaard

Department of Mathematics and Department of Mechanical Engineering, University of British Columbia, 2324 Main Mall, Vancouver, BC, Canada, V6T 1Z4.

Abstract

This paper describes a method for numerical solution of the flow equation for a Hele-Shaw model of displacement flow of non-Newtonian fluids in an eccentric annulus. The physical problem stems from an industrial process of oil well cementing during the well construction and successful mathematical modelling and solution of the problem can result in economic and environmental benefits. Here we outline the model for the displacement which uses the long-thin geometry of the annular domain to reduce the flow equations to two spatial dimensions. We proceed by putting the flow equation into its variation formulation and applying an iterative augmented Lagrangian algorithm to obtain a numerical solution. We examine convergence properties of the algorithm and its usefulness for practical applications.

Key words: Hele-Shaw cell, displacement flows, variational methods, augmented Lagrangian, visco-plastic fluid flow

1 Introduction

In construction of oil and gas wells it is necessary to cement a series of steel casings into the well as the depth increases. This is done both to support the wellbore and to provide zonal isolation throughout the length of the well, ensuring a hydraulic seal on the outside of the casing. The primary cementing process proceeds as follows, (1; 2). After a new section of the well is drilled, the drill pipe is removed from the wellbore, leaving the drilling mud behind.

A section of the steel casing is then inserted into the hole, leaving a small gap ($\sim$2 cm) between the outside of the casing and the rock, i.e. the annulus. Although centralizers are sometimes fitted to the outside of the casing to prevent the steel tubing from slumping to the lower side of the wellbore, it is very common that this annular gap is eccentred. After the casing is in place, a sequence of fluids is pumped down the inside of the tubing, reaching the bottom of the well and coming back up through the annular gap displacing the previous fluid. Typically, a wash or spacer fluid is pumped first, displacing the drilling mud left over both on the inside of the tubing and outside in the annulus, followed by one or more cement slurries. Drilling mud follows the final cement slurry pumped and circulation is stopped with a few meters of cement left at the bottom inside the casing. The cement is then allowed to set. Finally, the drilling resumes through the remaining part of cement inside the casing and further into the underlying rock.

A successful cement job results in removal of mud and spacer fluid from the annulus by the cement slurry. Unfortunately, mud is sometimes left behind in parts of the annulus and as the cement sets water is removed from it, producing a porous channel along which liquids and gasses from the surrounding rock formations can migrate upwards. This gas and fluid migration can result in negative safety and environmental consequences as well as loss of well productivity. In order to facilitate a successful mud removal it is possible to modify the rheologies and densities of the spacer fluid and the cement slurry together with the pumping rate within the constraints of maintaining well security. Here we focus on the laminar annular displacements which are used in the increasing number of wells and when the limitation of the pumping rates and outlying formation fracture pressure would not allow the use of the turbulent regime.

1.1 Modelling the process

The majority of the industrial literature on the subject of modelling the laminar displacement uses the hydraulic approach to the problem, leading to systems of design rules for a successful cementing job, (3; 4; 5; 6). These are applicable to mostly near-vertical wells and state that the flow should be sufficiently high to avoid a static mud channel on the narrow side of the annulus and there should be a positive gradient of rheological parameters and densities, so that each fluid is heavier than the one it displaces and generates higher frictional pressure. While such systems can be applied to good effect (7; 8), they tend to be conservative and experience problems with predicting flows in highly-deviated sections of the well. The other approach is to model the flow fully in 3-D (9; 10). It should be noted however that such an approach (e.g. using CFD software) is not practicable over the long scale of the wellbore

due to excessive computational requirements and is usually applied to selected cross-sections or simpler geometries. Here we follow an intermediate approach presented in (11) producing a flow model that allows for generality in terms of well geometry, inclination and fluid properties while at the same time reducing the problem to two dimensions thus significantly decreasing the computational load required to model displacements over the scale of the wellbore. We omit the detailed derivation and instead outline the key assumptions and resulting equations.

The flow is assumed to be laminar and incompressible with the fluids obeying the Herschel-Bulkley constitutive assumption. That is the relation between rate of stress τ and rate of strain $\dot{\gamma}$ is given by

$$\tau = \tau_Y + \kappa \dot{\gamma}^n \tag{1}$$

where τ_Y is the yield stress, κ is consistency and n is power law index of the fluid. The general idea is to use averaging in the radial direction across the annular gap in combination with scaling to reduce the three dimensional Navier-Stokes equations in cylindrical polar coordinates to two dimensions - axial and azimuthal. The key assumption enabling these simplifications is the narrowness of the annular gap that is typically a few centimeters compared with annular circumference ($\sim$ 1m.) and the axial length-scale of several hundred meters. We also assume homogeneity of the fluid across the annular gap - in effect we ignore the possibility that a layer of mud can remain stuck to the casing or the formation. Investigation of these effects by studying the displacements in a long axial section of the annulus is ongoing, (12; 13; 14; 15; 16). Also, only half of the annulus is considered, assuming that the flow is symmetric and the narrow side corresponds to its lowest part.

Dimensionless spatial coordinates are $(\phi, \xi) \in (0, 1) \times (0, Z)$. Here ϕ is the azimuthal coordinate with $\phi = 0$ denoting the wide side of the annulus and $\phi = 1$ the narrow (lower) side. The ξ coordinate measures axial depth upwards from bottom-hole $\xi = 0$ to the top of the zone of interest $\xi = Z$, where $Z \gg 1$. The annular half-gap width is denoted $H(\phi, \xi)$ and is (to the leading order):

$$H(\phi, \xi) = \bar{H}(\xi)(1 + e(\xi) \cos \pi\phi),$$

where $e(\xi) \in [0, 1)$ is the annular eccentricity with $e = 0$ corresponding to a concentric annulus. The mean annular radius at each depth is denoted by $r_a(\xi)$ and angle of inclination from the vertical $\beta(\xi)$. Throughout it is assumed that the annular geometry, (i.e. $\bar{H}(\xi)$, $r_a(\xi)$, $e(\xi)$ and $\beta(\xi)$) varies slowly with ξ.

The incompressibility condition for the flow is averaged across the annular

gap to remove the radial component and becomes

$$\frac{\partial}{\partial\phi}[H\overline{v}] + \frac{\partial}{\partial\xi}[Hr_a\overline{w}] = 0, \tag{2}$$

where $\overline{v}$ and $\overline{w}$ are the gap-averaged velocities in azimuthal and axial directions, respectively. This prompts definition of a stream-function Ψ:

$$\frac{\partial\Psi}{\partial\phi} = Hr_a\overline{w}, \qquad \frac{\partial\Psi}{\partial\xi} = -H\overline{v}. \tag{3}$$

A hydraulic argument is then made that the velocity field ($\overline{v}$, $\overline{w}$) is in the direction of the (modified) pressure gradient. Using the Herschel-Bulkley constitutive assumption this enables the determination of the relationship between the flow rate, the annular gap width $2H$ and the magnitude of the modified pressure gradient G, by considering Poiseuille flow between two parallel plates distance $2H$ apart:

$$|\nabla_a\Psi| = \begin{cases} 0 & \chi \le 0, \\ \dfrac{H^{m+2}}{\kappa^m(m+2)} \dfrac{\chi^{m+1}}{(\chi+\tau_Y/H)^2}\left[\chi + \dfrac{(m+2)\tau_Y}{(m+1)H}\right] & \chi > 0, \end{cases} \tag{4}$$

where $m = 1/n$ is the inverse power index for the fluid, $\chi = G - \tau_Y/H$ is the magnitude of pressure gradient above yield point (which is used instead of G to avoid singularity in the field equation) and $|\nabla_a\Psi|$ is the areal flow rate. The differential operators ∇_a and $\boldsymbol{\nabla}_a\cdot$ which are analogous to to the common gradient and divergence operators and are used to simplify the notation being defined as

$$\nabla_a q = \left(\frac{1}{r_a(\xi)}\frac{\partial q}{\partial\phi}, \frac{\partial q}{\partial\xi}\right), \qquad \boldsymbol{\nabla}_a\cdot\boldsymbol{q} = \frac{1}{r_a(\xi)}\frac{\partial q_\phi}{\partial\phi} + \frac{\partial q_\xi}{\partial\xi}.$$

The following system of two equations governing the annular displacement flow for a sequence of K fluids then results:

$$\frac{\partial}{\partial t}\left[Hr_a\bar{c}_k\right] + \frac{\partial}{\partial\phi}\left[H\overline{v}\ \bar{c}_k\right] + \frac{\partial}{\partial\xi}\left[Hr_a\overline{w}\ \bar{c}_k\right] = 0, \qquad k = 1, 2, ..., K \tag{5}$$

$$\boldsymbol{\nabla}_a\cdot\boldsymbol{S} = -f, \tag{6}$$

Here the first equation is referred to as advection equation and describes the time evolution of the (gap-averaged) concentration $\bar{c}_k$ of each fluid k in the sequence. In its derivation, the diffusive and dispersive effects have been ignored as they can be shown to be negligible compared with advection. The second equation is referred to as the field equation and coupled with the visco-plastic constitutive assumption

$$\boldsymbol{S} = \left[\frac{r_a\chi(|\nabla_a\Psi|)}{|\nabla_a\Psi|} + \frac{r_a\tau_Y}{H|\nabla_a\Psi|}\right]\nabla_a\Psi \Longleftrightarrow |S| > \frac{r_a\tau_Y}{H}, \tag{7}$$

$$|\nabla_a\Psi| = 0 \Longleftrightarrow |S| \leq \frac{r_a\tau_Y}{H}. \tag{8}$$

provides the stream function Ψ and thus the velocity field $(\overline{v}, \overline{w})$. In (7) the dependence of χ on $|\nabla_a\Psi|$ is calculated implicitly from (4). The buoyancy terms have been collected on the right hand side of (6) in the term f:

$$f = \boldsymbol{\nabla}_a \cdot \left(\frac{r_a\rho(\overline{\boldsymbol{c}})\cos\beta}{St^*}, \frac{r_a\rho(\overline{\boldsymbol{c}})\sin\beta\sin\pi\phi}{St^*}\right) = \boldsymbol{\nabla}_a \cdot \tilde{\boldsymbol{f}}, \tag{9}$$

where St^* is the global Stokes number for the flow. Finally, the boundary conditions for the concentration advection equation (5) are the symmetry of concentration at wide and narrow sides of the annulus together with $\overline{c}_k = 0$ or $\overline{c}_k = 1$ at $\xi = 0$, according to which fluid is entering the annulus. For the field equation (6) the boundary conditions are

$$\Psi(0, \xi, t) = 0, \qquad \Psi(1, \xi, t) = Q(t), \tag{10}$$

where $Q(t)$ is the imposed dimensionless flow rate. At the axial ends of the domain the Dirichlet conditions

$$\frac{\partial\Psi}{\partial\xi}(\phi, Z, t) = 0, \qquad \frac{\partial\Psi}{\partial\xi}(\phi, 0, t) = 0. \tag{11}$$

with the top- and bottom-end stream functions $\Psi_0(\phi, t) = \Psi(\phi, 0, t)$ and $\Psi_Z(\phi, t) = \Psi(\phi, Z, t)$ to be determined.

1.2 Existing methods of solution

The two resulting equations for the displacement flow (5) & (6) are at first sight in a suitable (decoupled) form for creating a numerical simulation of a flow. The field equation (6) allows us to calculate the fluid velocity given a specific concentration and the advection equation (5) specifies how to advance this concentration to the next time step using the computed velocity field. In fact, the advection equation is a standard conservation equation with the conserved quantity being $U = H\overline{c}_k$ and a great variety of suitable time-advance schemes exist for its numerical implementation. Solution of field equation (6) however presents a problem. It is a non-linear elliptic equation and in its classical formulation it is not necessarily well-defined due to the unyielded regions where $|S| \leq r_a\tau_Y/H$ being unspecified. And while it is possible to find analytic solutions for concentric annuli or perturbation solutions for cases with small annular eccentricity, so far we had to apply further simplifications to to the field equation to obtain a numerical solution for a general case.

One such approach described in (11) relies on using a perturbation method with small parameter $\varepsilon = 1/Z \ll 1$ and expanding the stream function Ψ in a regular perturbation series $\Psi = \Psi_0 + \varepsilon\Psi_1 + ...$ Upon substitution into (6), the field equation reduces to a series of one-dimensional boundary value problems that are solved on individual axial depth slices, that is for fixed values of ξ. To obtain a numerical solution for the resulting equations for Ψ_0 and Ψ_1, the function $[\chi(|\nabla_a\Psi|) + \tau_Y/H]/[|\nabla_a\Psi|/r_a]$ (as it appears in $\boldsymbol{S}$ in (7)) is regularized at $|\nabla_a\Psi| = 0$. Physically this implies making the effective viscosity of the fluids very large below their yield stress rather than infinite as prescribed by the constitutive equations.

Using this method for solution of the field equation is advantageous due to the fact that the length of the calculation scales linearly with the number of grid-points used to discretise the annulus and the numerical solution was found to be fast and robust. Coupled with a flux-corrected-transport (FCT) scheme for the solution of the advection equation, it enabled simulation of laminar displacement over the scale of the wellbore with sufficiently high speed and accuracy to be used in industrial applications. There are however several shortcomings of this numerical method. Firstly, the two-dimensional field equation (6) as derived in the model is not actually solved - only its perturbation approximation. Secondly, due to regularization of the constitutive equations at $|\nabla_a\Psi| = 0$ exact determination of mud channels, i.e. regions where the displaced fluid is unyielded and stationary is difficult.

Here we present a method utilizing an augmented Lagrangian algorithm for solution of variational elliptic equations, outlined in (17; 18). This method has been applied successfully in a simpler situation of one Bingham fluid flow in an annular cross-section in (19). Its application to our problem allows us to solve the field equation numerically as it is without any additional regularization or approximation. Implementation of this method makes it possible to test the validity of any of the simplified numerical simulations as well as being a valuable research tool by itself, enabling exact determination of the mud channels as predicted by the model. As the starting point we use the flow equations as described above in their variational formulation, which is derived in detail in (20) alongside several analytical results. Those of particular importance here apart from the variational formulation of the field equation are the formal proof of existence and uniqueness of its (weak) solution and derivation of analytical solution to the model for a concentric annulus.

2 Solution by augmented Lagrangian method

We begin by putting the the flow equation into its variational form and formulate it as a minimization problem:

$$Min_{v\in V_0}\{J(v)\}, \tag{12}$$

where

$$J(v) = F(\nabla_a v) + G(v), \text{ with} \tag{13}$$
$$F(q) = F_0(q) + F_1(q),\ q \in H, \text{ where} \tag{14}$$
$$F_0(q) = \int_\Omega \frac{r_a}{2} \int_0^{|\nabla_a \Psi^* + q|^2} \frac{\chi(s^{1/2})}{s^{1/2}}\ \mathrm{d}s\ \mathrm{d}\Omega,\ q \in H \tag{15}$$
$$F_1(q) = \int_\Omega \frac{\tau_Y r_a}{H} |\nabla_a \Psi^* + q|\ \mathrm{d}\Omega,\ q \in H \tag{16}$$
$$G(v) = -\int_\Omega fv\ \mathrm{d}\Omega,\ v \in V \tag{17}$$

In the above $\Omega = (0,1) \times (0,Z)$ is the domain considered with $\delta\Omega$ as its boundary and we homogenized the boundary conditions by setting

$$\Psi = \Psi^* + u,\ u \in C_0^2(\Omega) \tag{18}$$

with the suitably constructed Ψ^*. In (20) it is shown that this minimization problem has a unique solution in $W_0^{1,1+1/m}(\Omega)$ with $V_0 = W_0^{1,1+1/m}(\Omega)$ and $H = L^{1+1/m}(\Omega) \times L^{1+1/m}(\Omega)$. In the proofs of existence and uniqueness of the solution it is also shown that $F_0(q)$ is strictly convex and differentiable, $F_1(q)$ is convex and continuous and $G(v)$ is convex and continuous.

It should be noted that application of the augmented Lagrangian algorithm and associated convergence results require the solution space to be a Hilbert space and $W_0^{1,1+1/m}(\Omega)$ is only a Hilbert space for $m \leq 1$. It is more common however for the fluids used in primary cementing to be shear-thinning, that is with $m = 1/n > 1$. Nevertheless, once the variational problem has been approximated by a finite-dimensional numerical method (e.g. by finite volume method as we have done in practice), the approximate solution space V_h is finite dimensional - and thus is a Hilbert space. We hence take $V = H_0^1(\Omega)$ (so that $V_h \subset V$) and $H = L^2(\Omega) \times L^2(\Omega)$, making it possible to apply the existence and convergence theorems to the iterative solution of the approximate problem.

2.1 Principle of the method

A *Lagrangian functional* $\boldsymbol{L}$ associated with (13) is defined by

$$\boldsymbol{L}(v,q,\mu) = F(q) + G(v) + (\mu, \nabla_a v - q), \tag{19}$$

and for a given constant $r \geq 0$ an *augmented Lagrangian* $\boldsymbol{L}_r$ is defined by

$$\boldsymbol{L}_r(v,q,\mu) = \boldsymbol{L}(v,q,\mu) + \frac{r}{2}|\nabla_a v - q|^2 \tag{20}$$

Then, following Glowinski (18), it is true that $\{u,p,\lambda\}$ is a saddle point of $\boldsymbol{L}$ if and only if it is a saddle point of $\boldsymbol{L}_r,\ \forall r > 0$. Moreover such u is a solution of (12) and $p = \nabla_a u$. Thus finding the solution of the problem in its variational minimization formulation (12) is equivalent to finding saddle point of $\boldsymbol{L}_r$. This in turn is accomplished by an application of an iterative algorithm of Uzawa type: with $\lambda^n \in H\ \lambda^n \in H$ (and $\lambda^0 \in H$ given) known we find u^n, p^n, λ^{n+1} by solving

$$\boldsymbol{L}_r(u^n,p^n,\lambda^n) \leq \boldsymbol{L}(v,q,\lambda^n), \quad \forall \{v,q\} \in V \times H, \{u^n,p^n\} \in V \times H \tag{21}$$

$$\lambda^{n+1} = \lambda^n + \rho_n(\nabla_a u^n - p^n),\ \rho_n > 0. \tag{22}$$

Finding the solution of (21) is then equivalent to solving two coupled variational inequalities:

$$G(v) - G(u^n) + (\lambda^n, \nabla_a(v-u^n)) + r(\nabla_a u^n - p^n, \nabla_a(v-u^n)) \geq 0, \quad \forall v \in V, u^n \in V, \tag{23}$$

$$F(q) - F(p^n) - (\lambda^n, q-p^n) + r(p^n - \nabla_a u^n, q-p^n) \geq 0,\ \forall q \in H, p^n \in H. \tag{24}$$

The main drawback of this approach is that it requires solution of coupled variational inequalities at each step. To overcome this we uncouple the two inequalities in the natural way to obtain the following modified algorithm: with p^{n-1}, λ^n known ($p^0, \lambda^1 \in H$ given), we define u^n, p^n, λ^{n+1} by finding the solutions of:

$$G(v) - G(u^n) + (\lambda^n, \nabla_a(v-u^n)) + r(\nabla_a u^n - p^{n-1}, \nabla_a(v-u^n)) \geq 0, \quad \forall v \in V, u^n \in V, \tag{25}$$

$$F(q) - F(p^n) - (\lambda^n, q-p^n) + r(p^n - \nabla_a u^n, q-p^n) \geq 0,\ \forall q \in H, p^n \in H, \tag{26}$$

$$\lambda^{n+1} = \lambda^n + \rho_n(\nabla_a u^n - p^n),\ \rho_n > 0. \tag{27}$$

In fact the first step (solving (25)) corresponds to minimizing $\boldsymbol{L}_r(v, p^{n-1}, \lambda^n)$ with respect to v to get u^n and the second (solving (26)) to minimizing $\boldsymbol{L}_r(u^n, q, \lambda^n)$ with respect to q to obtain p^n.

2.2 Application of the algorithm

In application to our particular annular displacement problem with F and G as in (13 - 17) we have:

$$G(v) - G(u^n) + (\lambda^n, \nabla_a(v - u^n)) + r(\nabla_a u^n - p^{n-1}, \nabla_a(v - u^n)) \\ = \int_\Omega (-f - \nabla_a \lambda^n - r\boldsymbol{\nabla}_a \cdot (\nabla_a u^n - p^n))(v - u^n)\ \mathrm{d}\Omega. \tag{28}$$

Thus the first step of the algorithm (25) becomes finding the solution $u^n \in V$ to the Poisson equation

$$r\boldsymbol{\nabla}_a \cdot \nabla_a u^n = r\boldsymbol{\nabla}_a \cdot p^n - \nabla_a \lambda^n - f, \tag{29}$$

with the right hand side known at each iteration. For the second step we note that as we mentioned above, finding p^n at each step is equivalent to minimizing $\boldsymbol{L}_r(u^n, q, \lambda^n)$ with respect to q:

$$\begin{aligned} p^n &= \inf_q \{\boldsymbol{L}_r(u^n, q, \lambda^n)\} \\ &= \inf_q \{\int_\Omega (\frac{r_a}{2} \int_0^{|\nabla_a \Psi^* + q|^2} \frac{\chi(s^{1/2})}{s^{1/2}}\ \mathrm{d}s + \frac{\tau_Y r_a}{H} |\nabla_a \Psi^* + q| \\ &\quad + \frac{r_a}{2}|q|^2 - (\lambda^n + r\nabla_a u^n) \cdot q)\ \mathrm{d}\Omega\}. \end{aligned} \tag{30}$$

This minimization is achieved when p^n is given locally by:

$$\begin{aligned} p^n &= \inf_q \{\frac{r_a}{2} \int_0^{|\nabla_a \Psi^* + q|^2} \frac{\chi(s^{1/2})}{s^{1/2}}\ \mathrm{d}s + \frac{\tau_Y r_a}{H} |\nabla_a \Psi^* + q| \\ &+ \frac{r_a}{2}|\nabla_a \Psi^* + q|^2 - (\lambda^n + r\nabla_a u^n + r\nabla_a \Psi^*) \cdot (\nabla_a \Psi^* + q)\}. \end{aligned} \tag{31}$$

The expression above is minimized when $(\lambda^n + r\nabla_a u^n + r\nabla_a \Psi^*)$ is parallel to $\nabla_a \Psi^* + q$, since apart from the last term, the rest of the expression is a function of $|\nabla_a \Psi^* + q|$ only, i.e. independent of its direction. So, letting

$$\nabla_a \Psi^* + q = \theta(\lambda^n + r\nabla_a u^n + r\nabla_a \Psi^*), \tag{32}$$

$$x = |\lambda^n + r\nabla_a u^n + r\nabla_a \Psi^*| \tag{33}$$

we have to find the minimizer of

$$M(\theta) = \frac{r_a}{2} \int_0^{(\theta x)^2} \frac{\chi(s^{1/2})}{s^{1/2}}\ \mathrm{d}s + \frac{\tau_Y r_a}{H} |\theta| x + \frac{r_a}{2}(\theta x)^2 - \theta x \tag{34}$$

We now consider two cases: first, if $x \leq \tau_Y r_a / H$ then $\theta = 0$ minimizes M, giving $p^n = -\nabla_a \Psi^*$ (which corresponds to an "unyielded" flow at that point

for that iteration). If $x > \tau_Y r_a/H$ then we find θ by setting $\partial M/\partial\theta = 0$ which gives

$$r_a\chi(\theta x) + \frac{\tau_Y r_a}{H} + r\theta x - x = 0 \tag{35}$$

This can be inverted numerically to produce θ and whence p^n.

3 Application and results

Summarizing, the algorithm resulting from the application of the augmented Lagrangian method to the variational formulation is as follows: with p^{n-1}, λ^n known (p^0, $\lambda^1 \in H$ set), we find u^n, p^n, λ^{n+1} from

$$r\boldsymbol{\nabla}_a \cdot \nabla_a u^n = r\boldsymbol{\nabla}_a \cdot p^n - \nabla_a\lambda^n - f,\ u^n \in V, \tag{36}$$

$$p^n = \begin{cases} -\nabla_a\Psi^* & \text{if } x \le \frac{\tau_Y r_a}{H} \\ \theta(\lambda^n + r\nabla_a u^n + r\nabla_a\Psi^*) - \nabla_a\Psi^* & \text{if } x > \frac{\tau_Y r_a}{H} \end{cases} \tag{37}$$

$$\lambda^{n+1} = \lambda^n + \rho_n(\nabla_a u^n - p^n),\ \rho_n > 0. \tag{38}$$

where

$$x = |\lambda^n + r\nabla_a u^n + r\nabla_a\Psi^*|, \text{ and} \tag{39}$$

$$r_a\chi(\theta x) + \frac{\tau_Y r_a}{H} + r\theta x - x = 0, \tag{40}$$

with $V = H_0^1(\Omega)$ and $H = L^2(\Omega) \times L^2(\Omega)$, $\Omega = (0,1) \times (0,Z)$ and the relation between the modified pressure gradient χ and the flow rate $|\nabla_a\Psi|$ as in (4).

The result of solution of the algorithm is a sequence of functions u^n converging to $u \in H_0^1(\Omega)$ with the stream function $\Psi = \Psi^* + u$. We also obtain $p^n \in L^2(\Omega) \times L^2(\Omega)$ converging to $p = \nabla_a u$ from which the components of the velocity vector to be used in the concentration-advance equation can be easily calculated.

3.1 Numerical implementation

Our aim was to test the algorithm, its convergence properties and obtain a few results that can be compared to the analytical solutions in simple cases. As such, a very straight-forward finite volume discretization with a fixed regular rectangular mesh was chosen. That is we divide the domain Ω into $N_i \times N_j$ control volumes with each control volume being a rectangle of width $\Delta\phi = 1/N_i$ in the ϕ-direction and height $\Delta\xi = 1/N_j$ in the ξ-direction. Denoting by $CV_{i,j}$ the control volume with its lower left-hand corner at coordinates $(i\Delta\phi, j\Delta\xi)$, we define the discretized functions u_h^n, Ψ_h^n at the corners of $CV_{i,j}$ and the

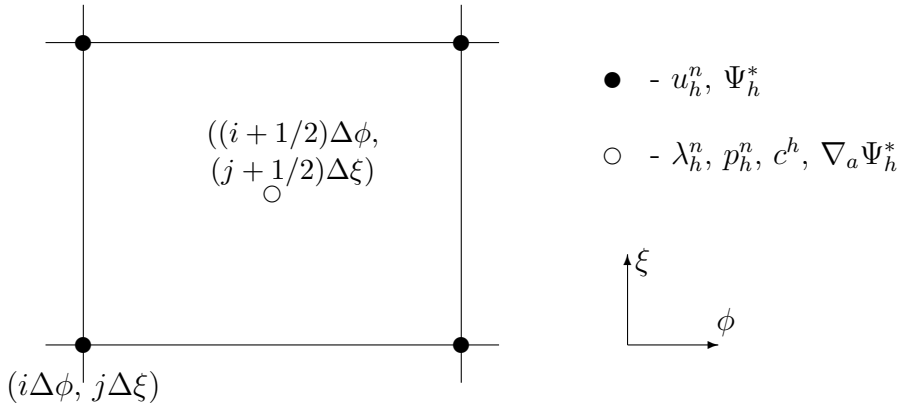

Fig. 1. Schematic picture of the control volume $CV_{i,j}$.

discretized functions λ_h^n, p_h^n and concentration c^h at its center - see Fig 1. This allows simplified calculation of gradients arising in the above equations as well as smaller spatial support of the numerical schemes for the chosen second degree of accuracy in each of the numerical calculations of the flux between the control volumes in the time-advance equation. Before the start of the iterative algorithm, we determine the homogenizing stream function Ψ_h^* by setting $\Psi_h^* = (1-c^h)\Psi_0^h + c_h \Psi_Z^h$. Here Ψ_0^h and Ψ_Z^h are the discretized stream functions at $\xi = 0$ and $\xi = Z$ correspondingly. They in turn are determined from the boundary conditions (11) which give the modified pressure gradient $G = \chi + \tau_Y / H$ constant in the ϕ-direction at the top and bottom of the well. Thus, χ at $\xi = 0$ and $\xi = Z$ can be calculated by numerically inverting the expression for the imposed rate of flow through the annulus.

At each iteration of the algorithm we first solve the u_h^n advance equation (36). We apply the standard point Gauss-Seidel method with second-order accurate spatial fluxes to solve this modified Poisson's equation. This seems especially appropriate as u_h^n converges after some iterations of the algorithm and so taking u_h^{n-1} as starting point of Gauss-Seidel iterations each time improves the convergence time. The same is true after application of the time-advance scheme: we then take the final value of u_h^n at the previous time-step as the starting point for Gauss-Seidel iterations. Over-relaxation was also used to improve the speed of convergence even further.

The second step in the algorithm is the advance of p_h^n. We achieve this by first calculating x from (39), determining if the fluid is yielded at that point and if so performing the numerical inversion in (40) to determine θ and thus p_h^n. Note that (40) can be differentiated analytically and a Newton-Raphson method used in its inversion converges in few iterations to the desired tolerance in most cases.

3.2 Convergence of the algorithm

Following Glowinski (18) we have $u_h^n \to u_h$ strongly in $V$where $u_h = \Psi_h - \Psi_h^*$ is the solution of the discretized minimization problem (12) producing the stream function Ψ_h solving the variational formulation of the flow equation. Also, $p_h^n \to p_h$ and H and $\lambda_h^{n+1} - \lambda_h^n \to 0$ strongly in H. From the λ-advance equation (38) this gives $p_h^n \to p_h = \nabla_a u_h = (H\bar{v_h},\ H\bar{w_h}) - \nabla_a \Psi_h^*$ in the discretized space.

We take the norm of $\Delta p_h^n = p_h^{n+1} - p_h^n$ as the measure of convergence of the numerical algorithm. This appears appropriate as it is the velocity field obtained directly from p_h^n that is used in the subsequent concentration advance step. Here we consider two norms of Δp_h^n: $L^2(\Omega)$ and $L^\infty(\Omega)$. While the first provides an adequate measure of convergence to the solution over the whole domain, the second gives a better impression about the convergence near the interface and yield boundaries - where it is the slowest. It should be noted that convergence of other quantities such as $\Delta\lambda_h^n = \lambda_h^{n+1} - \lambda_h^n$ and the residual from the flow equation $Res = \boldsymbol{\nabla}_a \cdot \boldsymbol{S}_h^n + f_h$ (where $\boldsymbol{S}_h^n$ and f_h are defined as in (7 - 9)) mirrors that of Δp_h^n.

The plots in Fig. 2 are of the logarithm base 10 of the L^2 and L^∞ norms of Δp_h^n versus the number of iterations together with surface plot of Δp_h^N after 100 iterations. In the three series of plots provided all of the parameters are the same except for the eccentricity. Here and in other cases we can observe that the algorithm converges better for lower eccentricity and when the fluid is yielded everywhere.

3.3 Steady states

We now combine the solution of the flow equation by augmented Lagrangian algorithm and a time-advance scheme for advection of the fluid concentrations according to (5) to produce a fully 2-D flow simulation. For the time-advance, we use a Flux Corrected Transport scheme which combines low-order (donor cell) and high-order (central difference) schemes to minimize the numerical dispersion and diffusion during the advection. It preserves the concentration jump at the interface between the fluids and was found to work well in application to the similar numerical computation performed in (11).

To validate and test the resulting simulation we can examine the steady interface shape development and propagation through the annular domain. Existence of such steady state displacements was shown in (20) and the shape of the steady-state interface in the case of a concentric annulus was derived

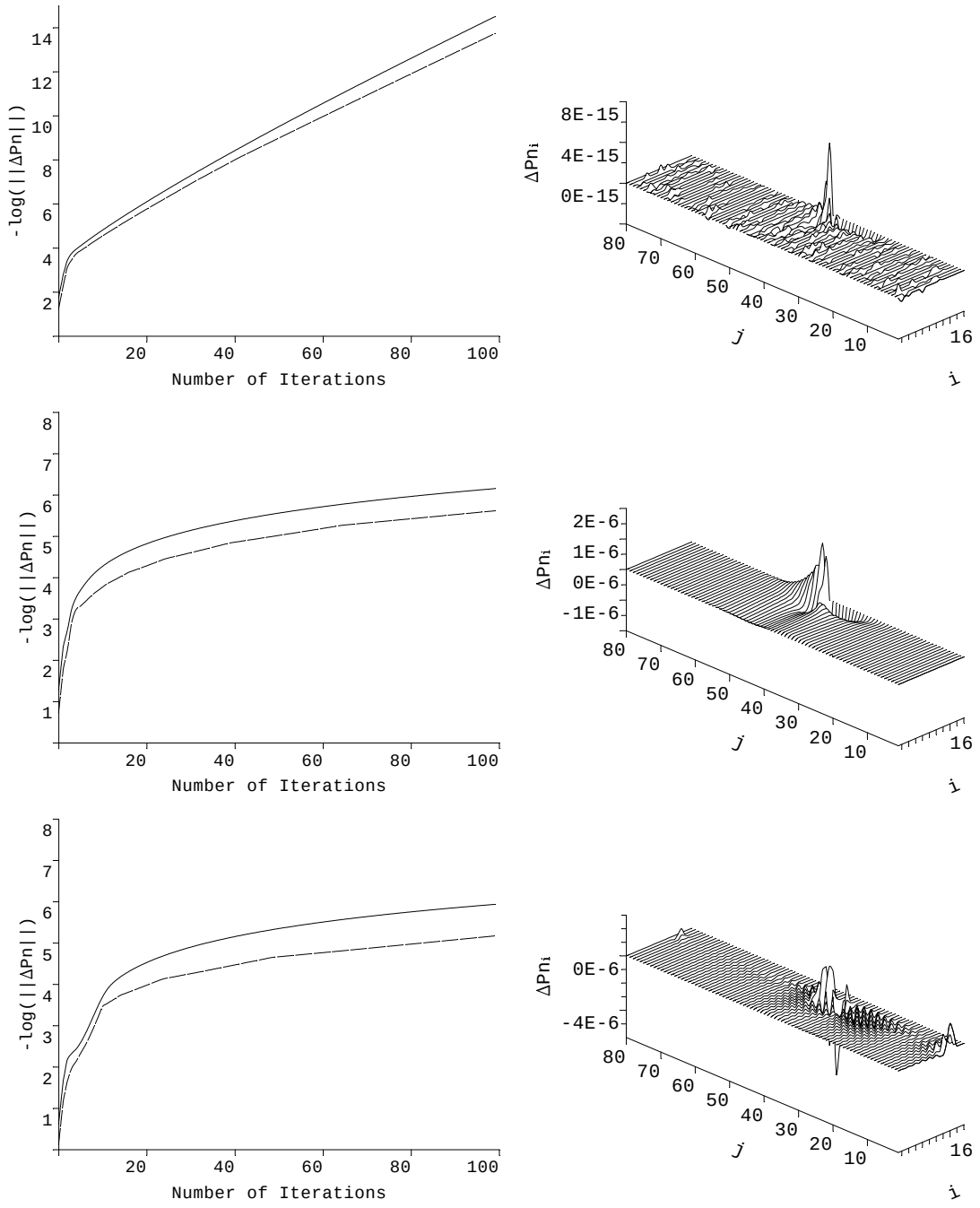

Fig. 2. Plot of Log_{10} of the L^2 (solid line) and L^∞ (broken line) norms of Δp_h^n against the number of iterations together with surface plots of the ϕ-component of ΔPU after 100 iterations (top to bottom): a) horizontal interface with $e = 0.1$, b) horizontal interface with $e = 0.6$, c) slanted interface with $e = 0.8$ and high yield stress of the displaced fluid.

analytically. The procedure we follow here is to set up an initial concentration field corresponding to a horizontal interface between two fluids in the middle of the domain. We then let the simulation run and the interface evolve, tracking its position on the wide side of the annulus. We also "follow the interface" by shifting the concentration field down at the average speed of the flow, thus keeping the interface centered in the domain. This allowed us to limit the axial

length of the grid to just a few annular diameters either side of the interface thus greatly reducing the computational load.

The results of the simulations are presented in Fig. 3, where we give the plot of the interface at the end of the simulation together with the time track of the inetrface position on the wide side of the annulus. The interface is taken to be the countour $c_h = 0.5$ and we use a 20×80 mesh with rectangular control volumes of width $\Delta\phi = 0.05$ in the ϕ-direction and of height $\Delta\xi = 0.1$ in the ξ-direction. We pick the length of a time-step Δt from the Courant-Friedrichs-Lewy (CFL) stability condition. The top plot corresponds to a vertical well where the interface stays horizontal. The second is for a horizontal well, where (from (20)) the steady-state interface is given by

$$g(\phi) = \frac{\rho_2 - \rho_1}{\chi_2(1) + \tau_{Y,2} - \chi_1(1) - \tau_{Y,1}} \cos(\pi\phi)/(\pi St^*). \tag{41}$$

The bottom plot is for an inclined well ($\beta = 5\pi/12$) with fluids of identical rheologies but a non-zero density difference, where the steady-state interface is given by $g(\phi) = -\tan\beta\cos(\pi\phi)/\pi$. In all of the cases the simulation converges to the interface shape predicted analytically and the average position of the interface on the wide side agrees with the analytical result.

3.4 Mud channels

4 Discussion and conclusion

In this paper we have described successful application of the iterative augmented Lagrangian algorithm to the problem of annular displacement of non-Newtonian fluids. The algorithm allows us to produce a numerical solution of the 2-D flow equation and can be used to create a simulator for the flow. While the implementation presented here was primarily for the purpose of validation of the algorithm, we can draw several conclusions about the possible use of such method. Firstly the method is stable for a very wide range of fluid rheologies, annular geometries and other parameters. While it suffers from the few limitations of the flow model it is based on, it makes no further simplifications and can be applied in the same generality of situations as the model itself. This makes it of special interest for the purposes of the model validation when combined with experimental data. It also allows verification of the simplified numerical simulations based on the same model.

The primary limitation of the method is the computational speed. For a 20×80 mesh considered here, a short flow simulation lasting 30 time units (equivalent to 3000 time steps of length 0.01 obtained from the CFL condition) can

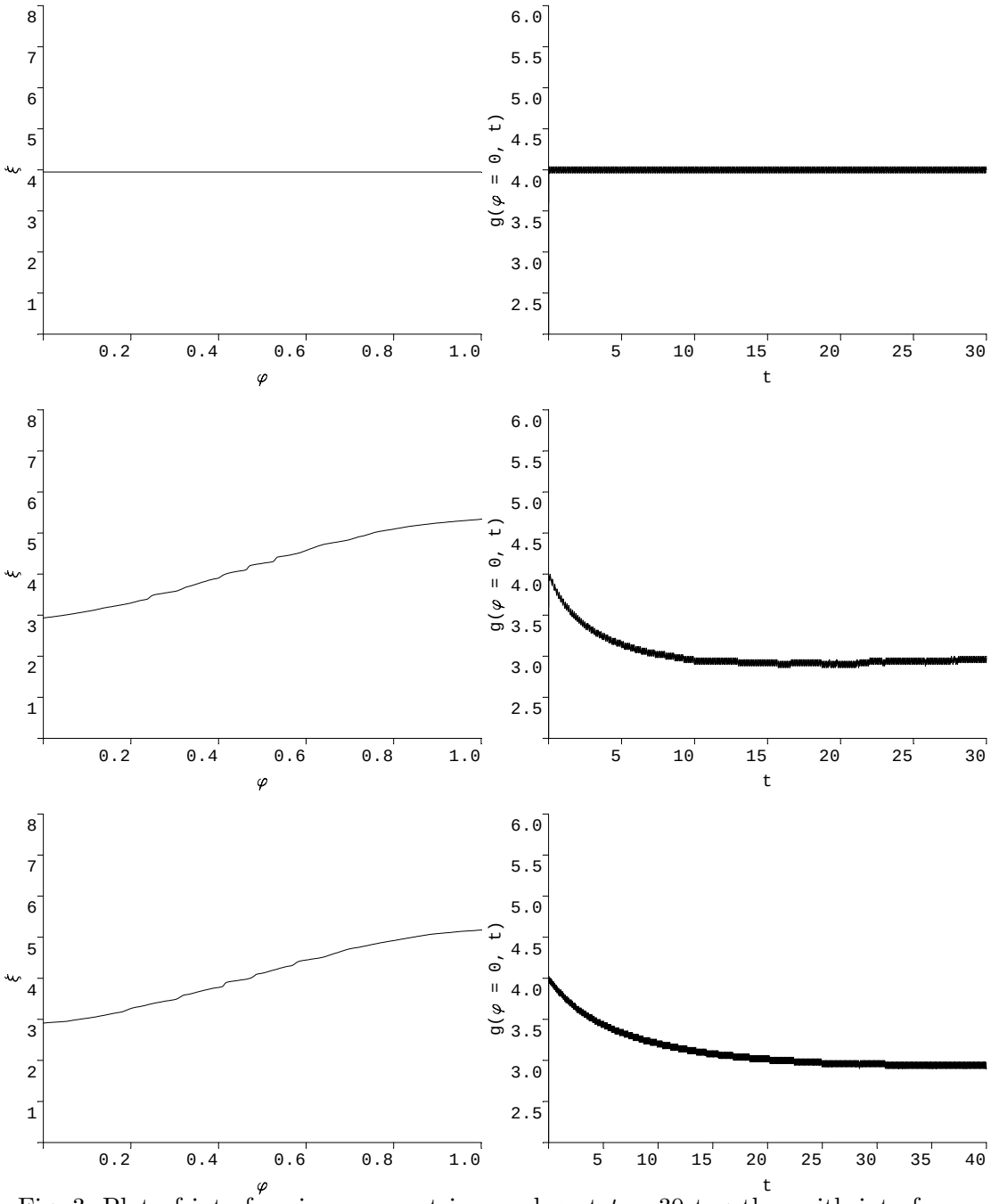

Fig. 3. Plot of interface in a concentric annulus at $t = 30$ together with interface track at $\phi = 0$ (top to bottom): a) vertical well $\beta = 0$ ($e = 0$; $\rho_1 = 1$; $\rho_2 = 0.6$; $\tau_{Y1} = 1$; $\tau_{Y2} = 0.8$; $k_1 = 1$; $k_2 = 0.8$), b) horizontal well $\beta = \pi/2$ ($e = 0$; $\rho_1 = 1$; $\rho_2 = 0.6$; $\tau_{Y1} = 1$; $\tau_{Y2} = 0.8$; $k_1 = 1$; $k_2 = 0.8$), c) inclined well with angle of inclination $\beta = 5\pi/12$ and identical rheologies ($e = 0$; $\rho_1 = 1$; $\rho_2 = 0.8$; $\tau_{Y1} = 1$; $\tau_{Y2} = 1$; $k_1 = 1$; $k_2 = 1$). Inverse power index $m_1 = m_2 = 1.0$ throughout.

take several hours on a current mid-range PC. This restricts the use of the method to smaller domains and shorter simulation times - such as for example experimental set ups. For full-scale industrial application with very long axial scale and running time, simplified methods such as the one described in (11) are of more use. Nevertheless, the speed of the iterative algorithm can be improved by the implementation of more efficient numerical methods, use of

the over-relaxation parameters ρ_n and r and considering a non-regular mesh to reduce the number of control volumes needed.

Another application of the algorithm with minimal alterations could be to laminar flow of non-Newtonian fluids through porous media - the problem occurring in the context of oil well stimulation amongst others. The underlying flow equations are very similar - in fact the first appearance (21) of the idea behind the Hele-Shaw displacement model considered here was deriving from the porous media flow analogy. For porous flows the ability of the method to predict the regions of unyielded fluids unambiguously would be most beneficial.

References

[1] E.B. Nelson. *Well Cementing.* Schlumberger Educational Services, (1990).

[2] C.W. Sauer. *Mud displacement during cementing: A state of the art.* Journal of Petrolium Technology, pages 1091-1101, September (1987).

[3] A. Jamot. *Displacement de la boue par le latier de ciment dans l'espace annulaire tubage-paroi d'un puits.* Revue Assoc. Franc. Techn. Petr., 224, pp.27-37, (1974).

[4] C.F. Lockyear and A.P. Hibbert. *Integrated Primary Cementing Study Defines Key Factors for Field Success.* Journal of Petrolium Technology, December (1989).

[5] C.F. Lockyear, D.F. Ryan and D.F. Gunningham. *Cement Channeling: How to Predict and Prevent.* Society of Petrolium Engineers, Paper number SPE 19865, (1989).

[6] M. Couturier, D. Guillot,H. Hendriks and F. Callet. *Design Rules and Associated Spacer Properties for Optimal Mud Removal in Eccentric Annuli.* Society of Petrolium Engineers, Paper number SPE 21594, (1990).

[7] S. Brady, P.P. Drecq, K.C. Baker, D.J. Guillot. *Recent Technological Advances Help Solve Cement Placement Problems in Gulf of Mexico.* Society of Petrolium Engineers, Paper number IADC SPE 23927, (1992).

[8] V.C. Kellessidis, R. Rafferty, A. Merlo, R. Maglione. *Simulator Models U-tubing to improve promary cementing.* Oil and Gas Journal, March (1994).

[9] N.A. Barton, G.L. Archer and G.L. Seymour. *Computational fluid dynamics improves liner cementing operation.* Oil and Gas Journal, September (1994).

[10] E.H. Vefring, K.S. Bjorkevoll, S.A. Hansen, N. Sterri, O. Saevareid, O. Aas and O. Merlo. *Optimization of Displacement Efficiency During Primary Cementing.* Society of Petrolium Engineers, Paper number SPE 39009, (1997).

[11] S.H. Bittleston, J. Ferguson and I. Frigaard. *Mud removal and cement placement during primary cementing of an oil well; laminar non-Newtonian displacements in an eccentric Hele-Shaw cell.* J. Engng. Math., May (2001).

[12] M. Allouche, I.A. Frigaard and G. Sona. *Static wall layers in the displacement of two visco-plastic fluids in a plane channel.* J. Fluid Mech., 424, pp. 243-277 (2000).

[13] I.A. Frigaard, O. Scherzer and G. Sona. *Uniqueness and non-uniqueness in the steady displacement of two visco-plastic fluids.* ZAMM, 81(2), pp. 99-118 (2001).

[14] I.A. Frigaard, M. Allouche and C. Gabard. *Incomplete displacement of viscoplastic fluids in slots and pipes - implications for zonal isolation.* Society of Petrolium Engineers paper number: SPE 64998, February (2001).

[15] I.A. Frigaard, M. Allouche and C. Gabard. *Setting rheological targets for chemical solutions in mud removal and cement slurry design.* Journal of Petrolium Technology, August (2001).

[16] I.A. Frigaard, S. Leimgruber and O. Scherzer. *Variational methods and maximal residual wall layers.* Submitted to J. Fluid Mechanics, March (2002).

[17] M. Fortin and R. Glowinski. *Augmented Lagrangian Methods.* North-Hollan, (1983).

[18] R. Glowinski. *Numerical Methods for Nonlinear Variational Problems.* Springer-Verlag, (1983).

[19] R.R. Huilgol and M.P. Panizza. *On determination of the plug flow region in Bingham fluids through the application of variational inequalities.* J. Non-Newtonian Fluid Mech., 58, 1995.

[20] S. Pelipenko and I.A. Frigaard. *On steady state displacements in primary cementing of an oil well.* Submitted to J. Engng. Math., August (2002).

[21] M. Martin, M. Latil and P. Vetter. *Mud Displacement by Slurry During Primary Cementing Jobs - Predicting Optimum Conditions.* Society of Petrolium Engineers, Paper number SPE 7590, (1978).